Electronic Supplementary Information (ESI)

for

Safranin O-Functionalized Cuboid Mesoporous Silica Material for Fluorescent Sensing and Adsorption of Permanganate

Sobhan Chatterjee,[ab] Jianchun Qin,[a] Xiangshuai Li,[a] Feng Liang,*[a] Dhirendra K. Rai,[c] and Ying-Wei Yang*[ab]

[a]College of Chemistry and College of Plant Science, Jilin University, Changchun 130012, China

[b]The State Key Laboratory of Refractories and Metallurgy, School of Chemistry & Chemical Engineering, Wuhan University of Science and Technology, Wuhan 430081, China

[c]Discipline of Metallurgy Engineering and Materials Science, Indian Institute of Technology Indore, Simrol, Indore 453552, India

*Corresponding Author(s): feng_liang@wust.edu.cn (F.L.); ywyang@jlu.edu.cn (Y.-W.Y.)

Contents

1. PXRD of SiO_2 and SiO_2@SFNO material:

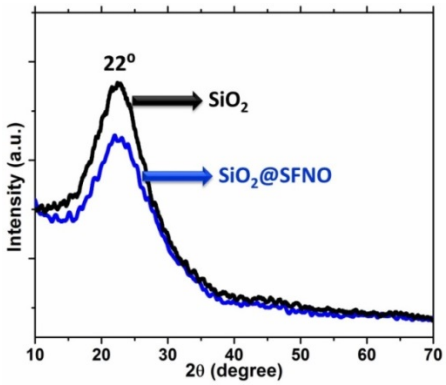

Fig. S1: Broad-angle powder X-ray diffractions pattern of SiO_2 and SiO_2@SFNO material.

2. Pore diameter of SiO_2 and SiO_2@SFNO material:

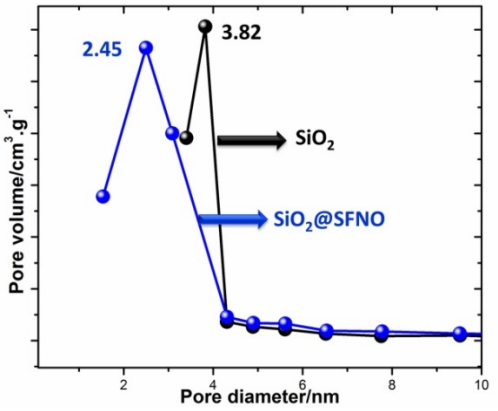

Fig. S2: Pore size distribution pattern of SiO_2 and SiO_2@SFNO material.

3. Table S1: Surface areas, pore volumes, and pore diameters of synthesize materials.

Materials	Surface area (m^2g^{-1})	Pore volume (cm^3g^{-1})	Pore diameter (nm)
SiO_2	463.6120	0.6370	3.82
SiO_2@SFNO	192.7490	0.0901	2.45

4. Solid state ^{29}Si CP (MAS) NMR of SiO_2 and SiO_2@SFNO material:

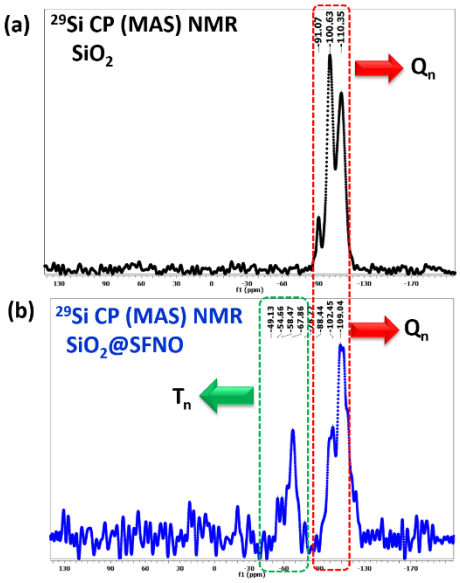

Fig. S3: Solid state ^{29}Si CP (MAS) NMR of **(a)** SiO_2 **(b)** SiO_2@SFNO.

5. CO_2-adsorption isotherms:

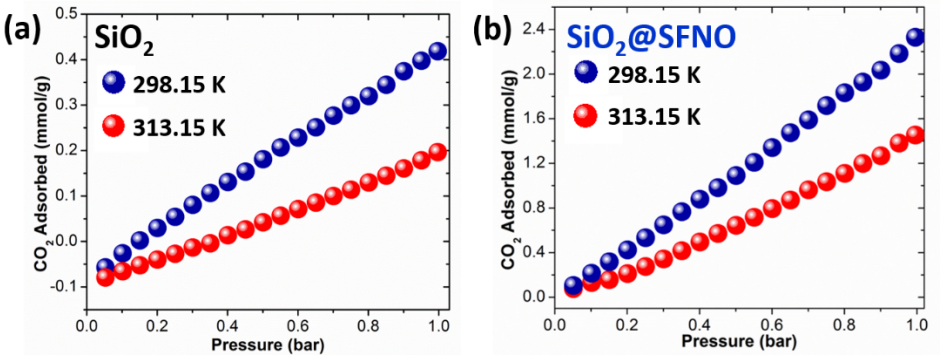

Fig. S4: CO_2-adsorption of **(a)** SiO_2 and **(b)** SiO_2@SFNO at 298.15 K and 313.15 K.

6. Table S2: CO_2 Uptake amount at 298.15 K and 313.15 K temperature.

Materials	298.15 K (mmol/g)	313.15 K (mmol/g)
SiO_2	0.4182	0.1963
SiO_2@SFNO	2.3480	1.4521

7. Limit of detection (LOD) calculation of SiO_2@SFNO towards MnO_4^-:

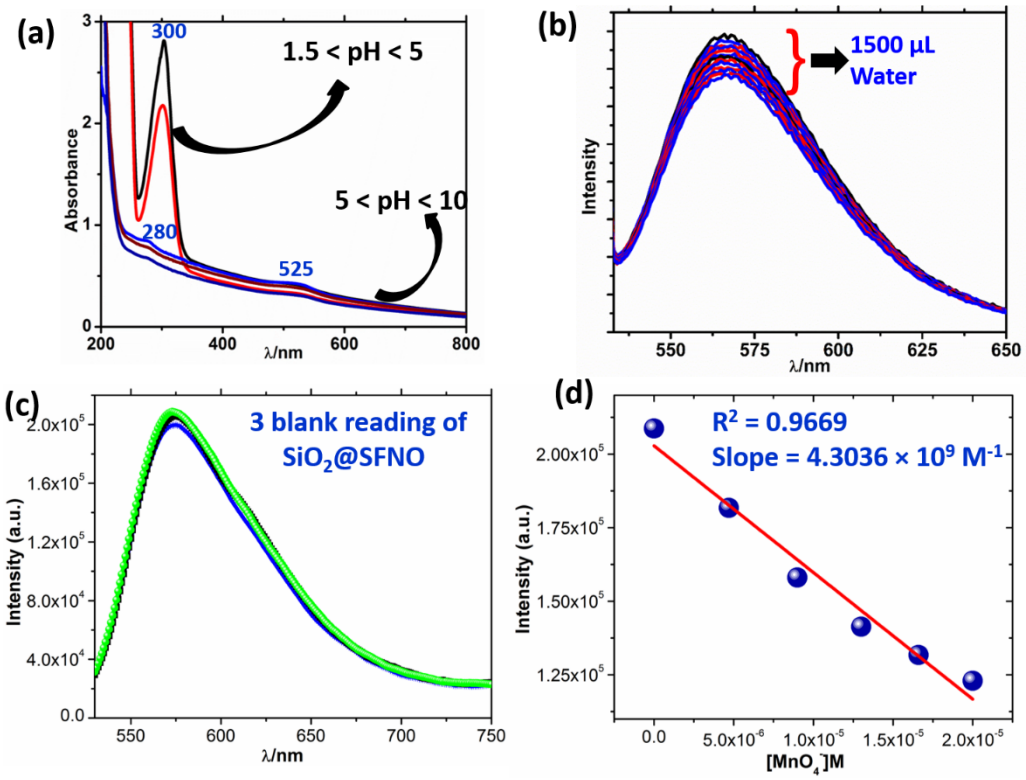

Fig. S5: (a) UV–Vis spectra of SiO_2@SFNO at different pH range. **(b)** SiO_2@SFNO titration against incremental addition of water (1.5 mL). **(c)**Three blank reading of suspended SiO2@SFNO material before MnO_4– titration. **(d)** Plot of fluorescence intensity vs concentration of MnO_4^-.

For determination of limit of detection (LOD), MnO_4^- (0 — 20 µM, 0 — 50 µL) was added to SiO_2@SFNO (2 mg/2 mL) and fluorescent intensity was recorded. By plotting fluorescence intensity with increasing concentration of MnO_4^- ions, slope (S) of graph was found to be 4.3036×10^9 M^{-1} with $R^2 = 0.9669$. Standard deviation (SD) was calculated from three blank reading of SiO_2@SFNO which is 968.1582. Detection limit is calculated according to the formula: Detection limit = (3SD/S).

Blank reading	Fluorescence Intensity
1.	208939
2.	208054
3.	207005
Standard deviation (SD)	968.1582

8. Table S3: Comparison of detection limits (LOD) and adsorption capacity of SiO_2@SFNO (organic-inorganic hybrid material) towards MnO_4^- with others material. (Other materials do not show dual-functional activities and in vivo application).

Material Type	Detection limit	Adsorption capacity	Dual functionality	In vivo detection	Reference
MOF	–	292 mg/g	No	No	[S1]
MOF	0.34×10^{-3} M	–	No	No	[S2]
MOF	0.28 μM	–	No	No	[S3]
MOF	398 ppb	–	No	No	[S4]
MOF	1.47×10^{-4} M	–	No	No	[S5]
MOF	3.38×10^{-4} M	–	No	No	[S6]
MOF	1.73×10^{-4} M	–	No	No	[S7]
MOF	1.0×10^{-4} M	–	No	No	[S8]
Polymer	–	94.4%	No	No	[S9]
Polymer	8.81 ppm	–	No	No	[S10]
Microgel	25 nM	–	No	No	[S11]
Organic–inorganic hybrid material	**67 ppb (5.58×10^{-7} M)**	**292 mg/g (98.50%)**	**Yes**	**Yes**	**This Work**

9. The adsorption performance of SiO_2@SFNO for MnO_4^- and Langmuir and Frundlich equation:

Batch adsorption experiments were performed in an aqueous MnO_4^- ($KMnO_4$) solution to calculate several adsorption parameters and adsorption isotherms. Adsorption capacity (Q_e) measurements for MnO_4^- were done by taking 5 mg of SiO_2@SFNO material in ten batches of 50 ml aqueous MnO_4^- solution of different concentration (10 ppm to 100ppm) by the using of equation: $q_e = (C_i - C_e)V/W$. In this equation, Q_e, C_i, and C_e represent the equilibrium adsorption capacity (mg/g), initial and equilibrium concentration of MnO_4^- aqueous solution (mg/L) respectively. Each batch containing a suspension of 5 mg SiO_2@SFNO in aqueous MnO_4^- solution was stirred at room temperature for 2h, after which, the concentration of unabsorbed MnO_4^- was determined from UV-Visible spectrum of the filtrate by comparing its UV-Visible spectrum with the calibration plot. All the adsorption experiments were repeated twice to remove the experimental error.

The Langmuir adsorption isotherm (mono layer adsorption) is represented in the equation $C_e/q_e = C_e/q_{max} + 1/q_{max} \times K_L$, where C_e is the equilibrium concentration of MnO_4^- (mg/L), q_e is the equilibrium adsorption capacity (mg/g), and K_L is the Langmuir adsorption constant. The possibility of multi-layer adsorption is allowed in Freundlich adsorption model, and it's represented in the equation $lnq_e = ln\, K_f + \frac{1}{n} lnC_e$, Where K_f and n are Freundlich constants related to adsorption capacity and adsorption intensity, respectively.

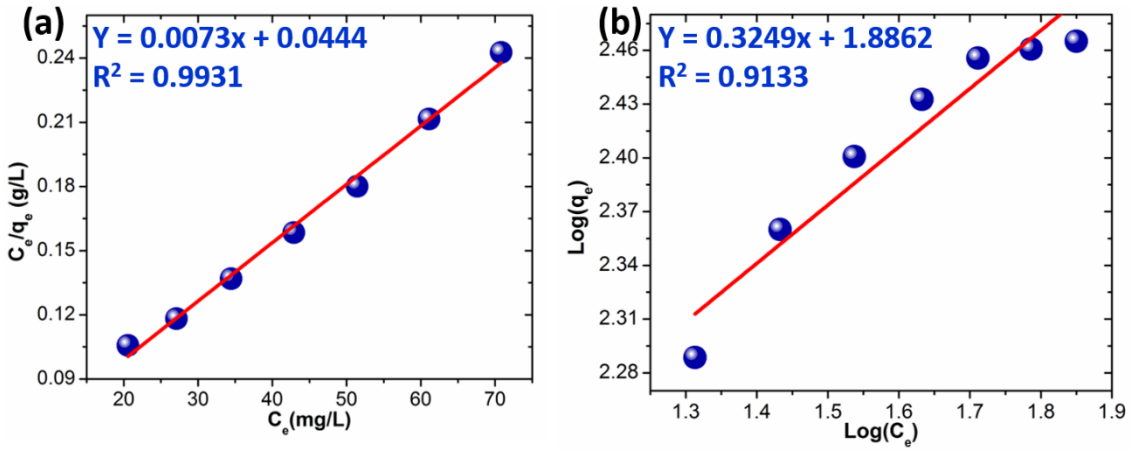

Fig. S6: (a) Langmuir and **(b)** Freundlich adsorption isotherm of MnO_4^- at room temperature.

10. Table S4: Langmuir and Freundlich parameter of SiO_2@SFNO towards MnO_4^-

Isotherm	Experimental q_m (mg/g)	Q_{max} (mg/g)	K_L (L/g)	R^2
Langmuir linear isotherm	292	370	0.0607	0.9931
Isotherm	Experimental q_m (mg/g)	K_F	n	R^2
Freundlich linear isotherm	292	77	3.0778	0.9133

11. Adsorption mechanism SiO_2@SFNO to MnO_4^-:

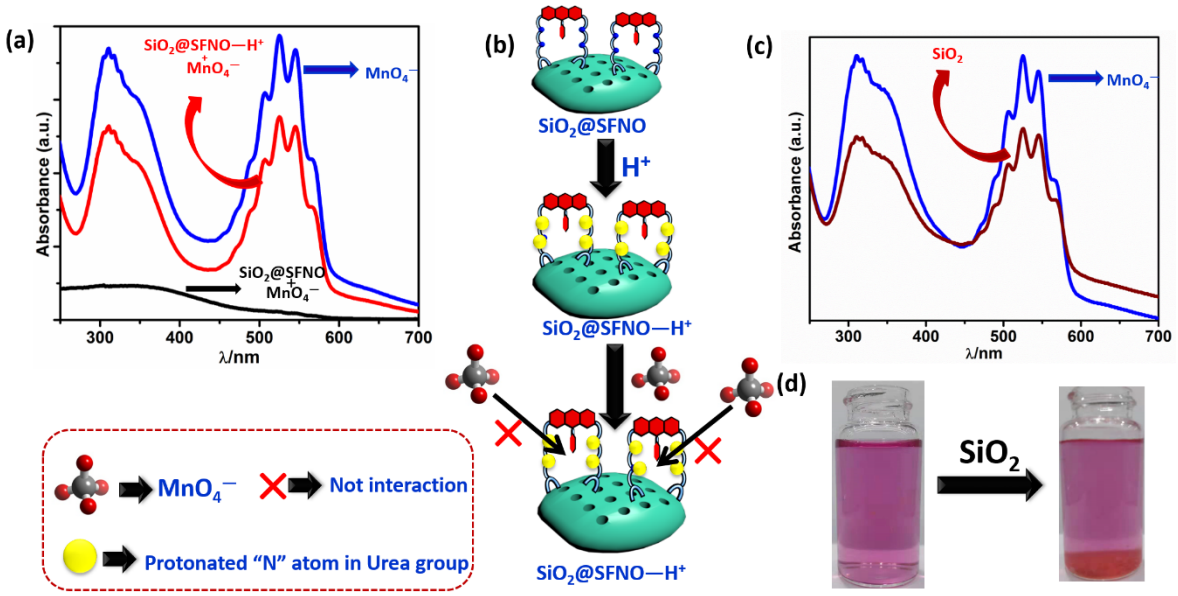

Fig. S7: Adsorption of MnO_4^- in presence of SiO_2@SFNO and acidified SiO_2@SFNO (SiO_2@SFNO–H^+). **(a)** UV-vis spectrum of MnO_4^- solution treated after SiO_2@SFNO and acidified SiO_2@SFNO. **(b)** Probable adsorption mechanism of SiO_2@SFNO. **(c)** Adsorption study of MnO_4^- in presence of SiO_2. **(d)** Real Photography of MnO_4^- in presence of SiO_2.

12. Fluorescence and Zeta potential change with incremental addition of acid:

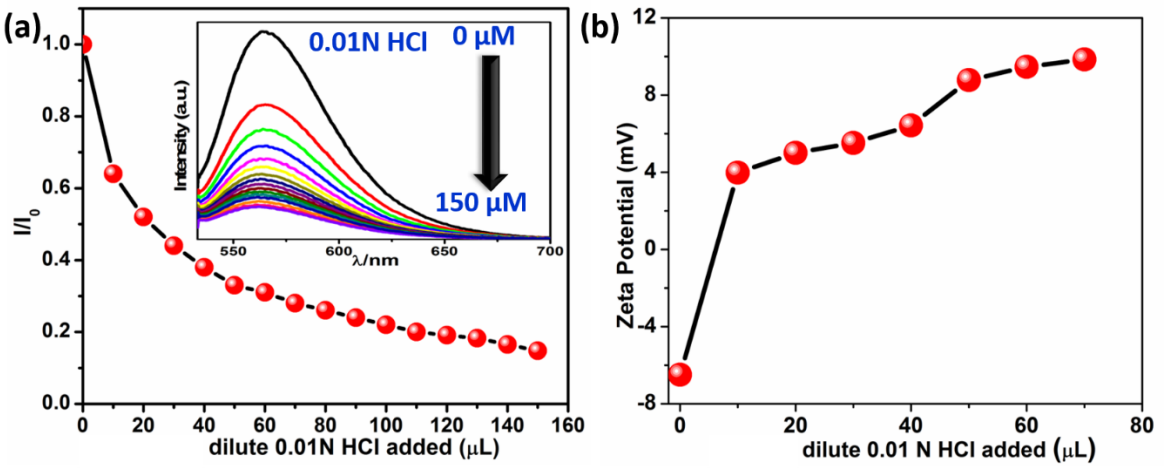

Fig. S8: (a) Fluorescence and **(b)** Zeta potential of SiO_2@SFNO changes with incremental addition of diluted 0.01 N HCl.

13. FT-IR and PXRD of MnO_4^-–SiO_2@SFNO complex:

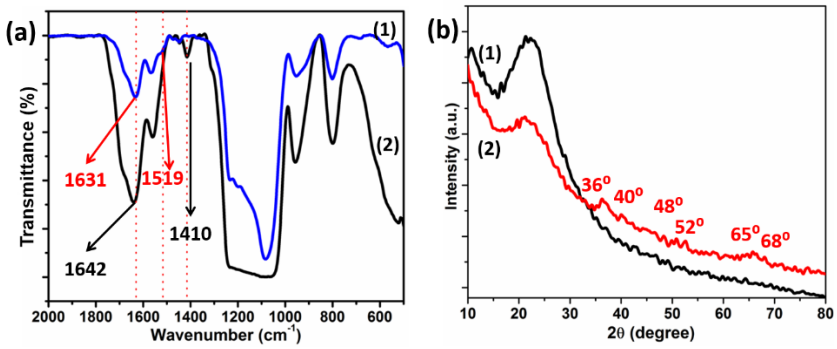

Fig. S9: (a) FTIR of 1) SiO_2@SFNO and 2) MnO_4^- loaded SiO_2@SFNO; **(b)** PXRD of 1) SiO_2@SFNO, and 2) MnO_4^- loaded SiO_2@SFNO.

14. EDX spectrum of MnO_4^- loaded SiO_2@SFNO:

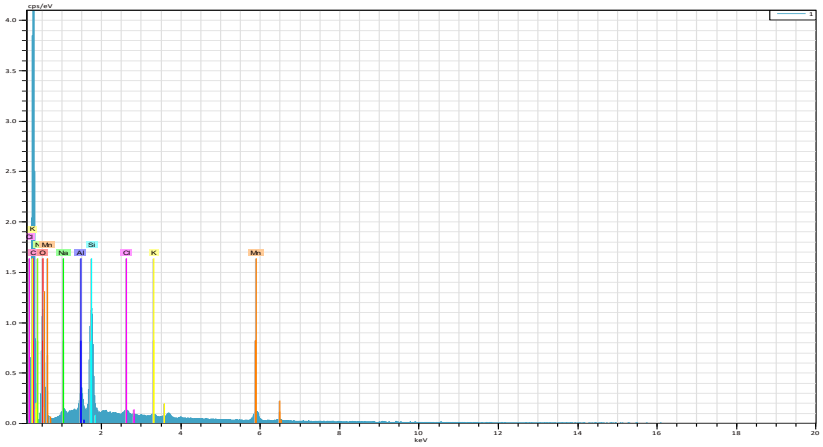

Fig. S10: EDX spectrum of MnO_4^-–SiO_2@SFNO.

15. B-H plot with fluorescence quenching data:

Though it is very difficult to provide any direct evidence of the binding mode of MnO_4^-, Hg^{2+}, and Cu^{2+} on the SiO_2@SFNO surface, an indirect method was established by Benesi-Hildebrand (B–H) fluorescence quenching equation. These B–H plots were used to determine the stoichiometry of the MnO_4^-–SiO_2@SFNO, Hg^{2+}–SiO_2@SFNO, and Cu^{2+}–SiO_2@SFNO complexes. In case of a 1:1 complex, the B-H equation is:

$$\frac{1}{F_o - F} = \frac{1}{(F_o - F_\infty).K.[M]} + \frac{1}{[F_o - F_\infty]}$$

In this approach, a linear plot will be get when $\frac{1}{F_o - F}$ is plotted against $\frac{1}{[M]}$

For 1:2 complexes, the B-H equation is:

$$\frac{1}{F_o - F} = \frac{1}{(F_o - F_\infty).K.[M]^{1/2}} + \frac{1}{[F_o - F_\infty]}$$

In this approach, a straight line will be get when $\frac{1}{F_o - F}$ is plotted against $\frac{1}{[M]^{1/2}}$

Where F is the detected fluorescence data of each titration, F_o is the fluorescence intensity of the SiO_2@SFNO in the absence of ions, F_α is the fluorescence intensity at saturation and [M] is denoted as concentration of ions.

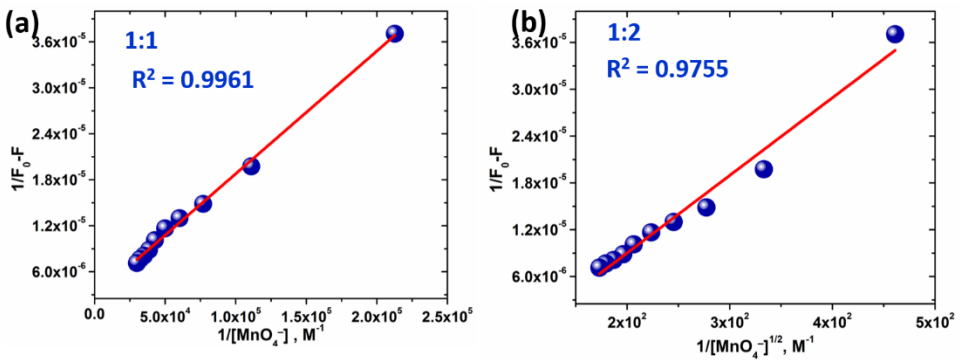

Fig. S11: Linear B–H plots indicating **(a)** 1:1 and **(b)** 1:2 complexation between MnO_4^- and SiO_2@SFNO.

16. LOD plots of SiO_2@SFNO towards Hg^{2+} and Cu^{2+}:

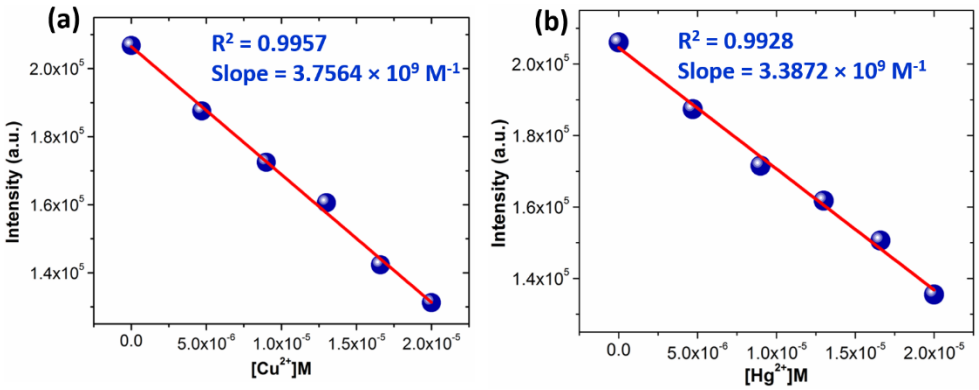

Fig. S12: Plotting fluorescence intensity with increasing concentration of **(a)** Cu^{2+} and **(b)** Hg^{2+}.

17. B–H plot of Cu^{2+}:

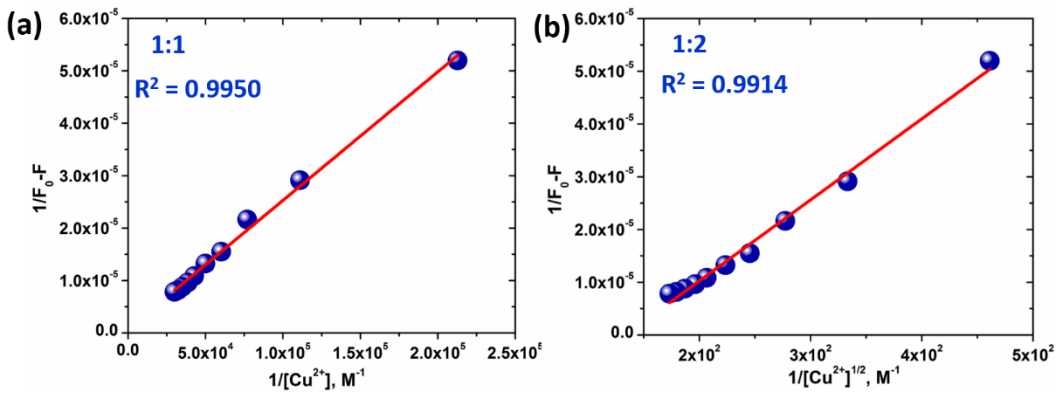

Fig. S13: Linear B–H plots indicating **(a)** 1:1 and **(b)** 1:2 complexation between Cu^{2+} and SiO_2@SFNO.

18. B–H plots of Hg^{2+}:

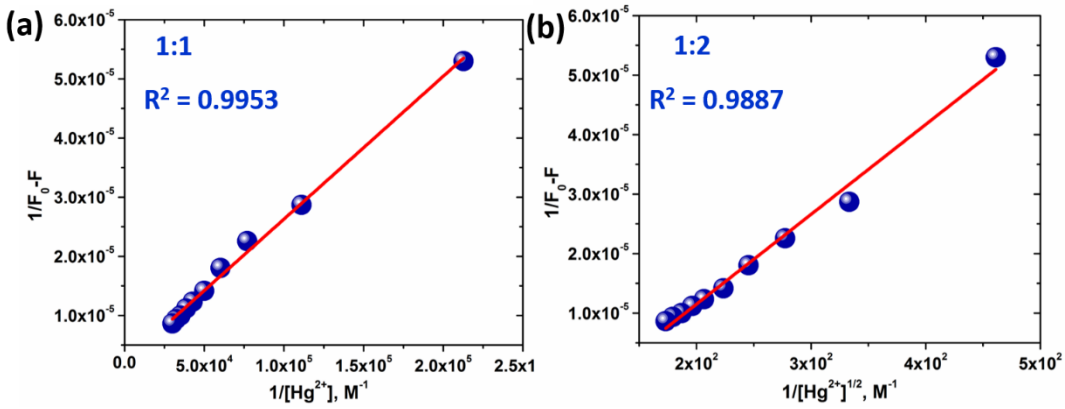

Fig. S14: Linear B–H plots indicating **(a)** 1:1 and **(b)** 1:2 complexation between Hg^{2+} and SiO_2@SFNO.

19. Broad angle PXRD of complex Cu^{2+}–SiO_2@SFNO, and Hg^{2+}–SiO_2@SFNO:

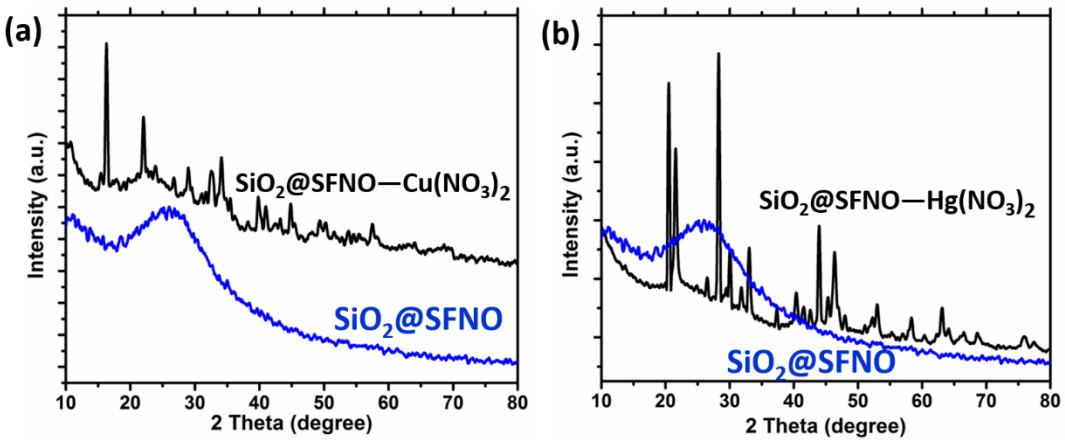

Fig. S15: PXRD of **(a)** Cu^{2+} and **(b)** Hg^{2+} loaded SiO_2@SFNO.

20. Plausible binding mechanism of SiO_2@SFNO towards MnO_4^-, Cu^{2+}, and Hg^{2+}:

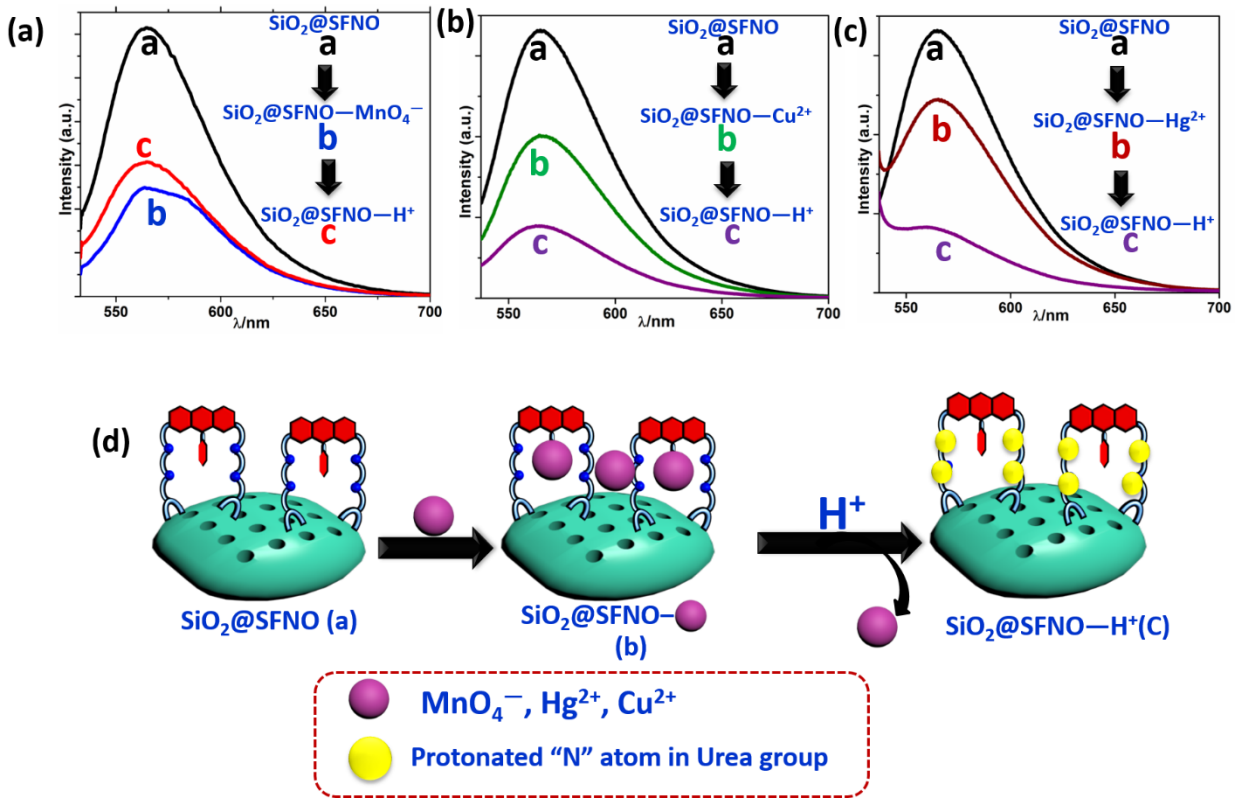

Fig. S16: Fluorescence spectra of SiO_2@SFNO in presence of **(a)** MnO_4^- + H^+, **(b)** Cu^{2+} + H^+, and **(c)** Hg^{2+} + H^+.

21. Fluorescence of SiO_2@SFNO with various excitation wavelengths:

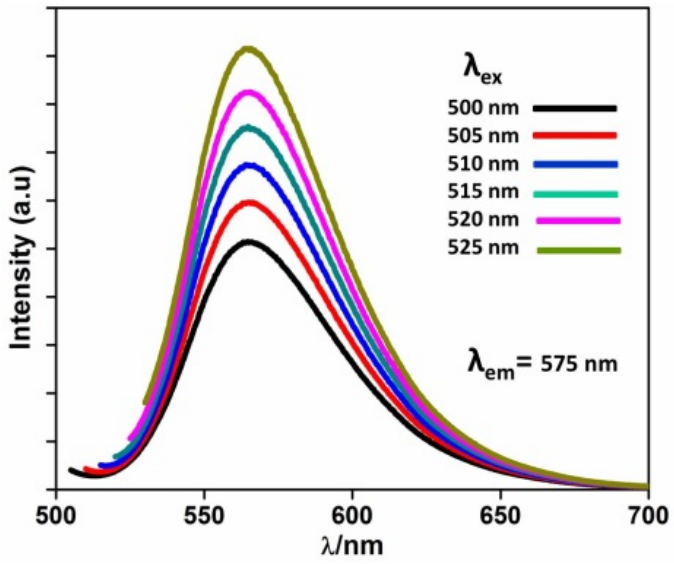

Fig. S17: Fluorescence spectral studies of SiO_2@SFNO (2 mg/2 mL in aqueous solution) with various excitation wavelengths.

22. Cu^{2+} and Hg^{2+} in vivo detection application:

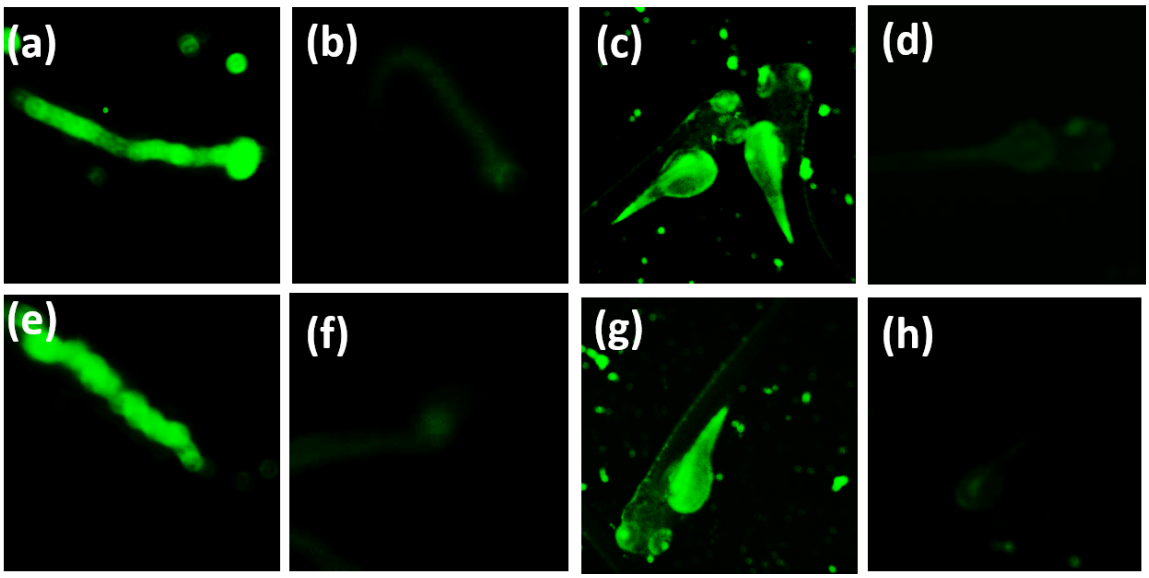

Fig. S18: Fluorescence imaging of limnodrilus claparedianus and six-day-old zebrafish incubated with SiO_2@SFNO (20 mL PBS saline, 100 µL from 20mg/20mL stock solution). Fluorescence images of limnodrilus claparedianus before (**a**) & **(e)** and after **(b)** & **(f)** incubated with Cu^{2+} (10×10^{-6} M) and Hg^{2+} (10×10^{-6} M) respectively. Fluorescence image of zebrafish before **(c)** & **(g)** and after **(d)** & **(h)** incubated with Cu^{2+} (10×10^{-6} M) and Hg^{2+} (10×10^{-6} M) respectively.

23. Mass spectral study of ligand SFNO:

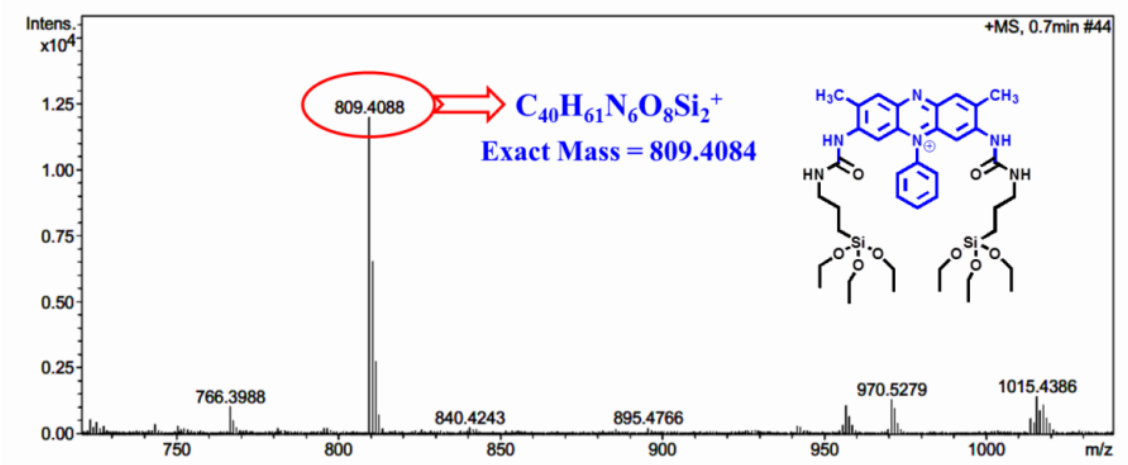

Fig. S19: ESI-MS spectra of ligand SFNO.

24. References

S1. Deng, S. Q.; Mo, X. J.; Zheng, S. R.; Jin, X.; Gao, Y.; Cai, S. L.; Fan, J.; Zhang, W. G. Hydrolytically Stable Nanotubular Cationic Metal-Organic Framework for Rapid and Efficient Removal of Toxic Oxo-Anions and Dyes from Water. *Inorg Chem* **2019**, *58*, 2899-2909.

S2. Chen, M.; Xu, W.-M.; Tian, J.-Y.; Cui, H.; Zhang, J.-X.; Liu, C.-S.; Du, M. A terbium(iii) lanthanide–organic framework as a platform for a recyclable multi-responsive luminescent sensor. *J. Mater. Chem. C* **2017**, *5*, 2015-2021.

S3. Ding, B.; Liu, S. X.; Cheng, Y.; Guo, C.; Wu, X. X.; Guo, J. H.; Liu, Y. Y.; Li, Y. Heterometallic Alkaline Earth–Lanthanide Ba^{II}–La^{III} Microporous Metal–Organic Framework as Bifunctional Luminescent Probes of Al^{3+} and MnO_4^-. *Inorg. Chem.* **2016**, *55*, 4391-4402.

S4. Jana, A. K.; Natarajan, S. Fluorescent Metal–Organic Frameworks for Selective Sensing of Toxic Cations (Tl^{3+}, Hg^{2+}) and Highly Oxidizing Anions ($(CrO_4)^{2-}$, $(Cr_2O_7)^{2-}$, $(MnO_4)^-$). *Chempluschem* **2017**, *82*, 1153-1163.

S5. Wu, J. X.; Yan, B. Eu(III)-Functionalized In-MOF (In(OH)bpydc) as Fluorescent Probe for Highly Selectively Sensing Organic Small Molecules and Anions Especially for $CHCl_3$ and MnO_4^-. *J. Colloid Interface Sci.* **2017**, *504*, 197-205.

S6. Yan, Y. T.; Zhang, W. Y.; Zhang, F.; Cao, F.; Yang, R. F.; Wang, Y. Y.; Hou, L. Four new metal–organic frameworks based on diverse secondary building units: sensing and magnetic properties. *Dalton Trans.* **2018**, *47*, 1682-1692.

S7. Wu, J. X.; Yan, B. Eu(III)-Functionalized In-MOF (In(OH)bpydc) as Fluorescent Probe for Highly Selectively Sensing Organic Small Molecules and Anions Especially for $CHCl_3$ and MnO_4^-. *J. Colloid Interface Sci.* **2017**, *504*, 197-205.

S8. Yang, S.-L.; Yuan, Y.-Y.; Sun, P.-P.; Lin, T.; Zhang, C.-X.; Wang, Q.-L. 3D water-stable europium metal organic frameworks as a multi-responsive luminescent sensor for high-efficiency detection of $Cr_2O_7^{2-}$, MnO_4^-, Cr^{3+} ions and SDBS in aqueous solution. *New J. Chem.* **2018**, *42*, 20137-20143.

S9. Chandra, D.; Bhaumik, A. A new functionalized mesoporous polymer with high efficiency for the removal of pollutant anions. *J. Mater. Chem.* **2009**, *19*, 1901-1907.

S10. Yao, S.-L.; Zheng, T.-F.; Tian, X.-M.; Liu, S.-J.; Cao, C.; Zhu, Z.-H.; Chen, Y.-Q.; Chen, J.-L.; Wen, H.-R. Dicarboxylate-induced structural diversity of luminescent Zn^{II}/Cd^{II} coordination polymers derived from V-shaped bis-benzimidazole. *CrystEngComm* **2018**, *20*, 5822-5832.

S11. Zhu, Z.; Xue, J.; Wen, B.; Ji, W.; Du, B.; Nie, J. Ultrasensitive and selective detection of MnO_4^- in aqueous solution with fluorescent microgels. *Sens. Actuators B Chem.* **2019**, *291*, 441-450.